Multiplicity of nonlinear thermal convection in a spherical shell

Ligang Li,[1] Pu Zhang,[1] Xinhao Liao,[2] and Keke Zhang[1,*]
[1]*Department of Mathematical Sciences, University of Exeter, Exeter EX4 4QE, United Kingdom*
[2]*Shanghai Astronomical Observatory, Shanghai 200030, China*
(Received 26 July 2004; published 4 January 2005)

Linear and weakly nonlinear thermal convection in a moderately thin spherical shell in the presence of a spherically symmetric gravity subject to a spherically symmetric boundary condition is systematically investigated through fully three-dimensional numerical simulations. The convection problem is self-adjoint and the linear convective stability is characterized by l, the degree of a spherical harmonics $Y_l^m(\theta,\phi)$. While the radial structure of the linear convection is determined by the stability analysis, there exists a $(2l+1)$-fold degeneracy in the horizonal structure of the spherical convection. When $l=O(10)$, i.e., in a moderately thin spherical shell, the removal or partial removal of the degeneracy represents a mathematically difficult, physically not well-understood problem. By starting with carefully chosen initial conditions, we are able to obtain a variety of nonlinear convective flows at exactly the same parameters near the onset of convection, including steady axisymmetric convection, steady azimuthally periodic convection, steady azimuthally nonperiodic convection, equatorially asymmetric convection, and steady convection in the form of a single giant spiral roll covering the whole spherical shell which is stable and robust for a wide range of the Prandtl number.

DOI: 10.1103/PhysRevE.71.016301 PACS number(s): 47.20.Bp, 47.54.+r, 47.27.Te

I. INTRODUCTION

The problem of thermal convection in a spherical fluid shell is of interest to geophysical and astrophysical fluid systems (e.g., [1–3]). At leading-order approximation, thermal convection in the Earth's mantle (a thick spherical shell) or in Mercury's mantle (a moderately thin shell) is subject to a spherically symmetric radial gravity force and a spherically symmetric boundary condition. It is generally accepted that planetary magnetic fields are generated through magnetohydrodynamic processes in their electrically conducting fluid cores below the planetary mantles. Paleomagnetic and historical magnetic field measurements suggest persistent distinct patterns of variation of the geomagnetic field taking place in different regions of the lower mantle [4]. There is strong evidence that the structure of the Earth's magnetic fields is strongly affected by the pattern of heat flux boundary conditions at the top of the fluid core which is associated with the pattern of the overlying mantle convection [5]. Similar effects would occur in other Earth-like planets. This is because lateral variations in heat flux across the core-mantle boundary drive flows in planetary cores which can significantly influence the generation process of planetary magnetic fields [6]. The problem of convection pattern in a spherical shell is hence closely linked to the thermal history of planets and their magnetic fields.

The convection problem in a spherical shell, particularly in a moderately thin shell, is marked by the pattern and orientational degeneracies (e.g., [7–10]). Here the pattern degeneracy is concerned with the exact same eigenvalue for many linear solutions which have different spatial structures on a spherical surface and are physically equally realizable, while the orientational degeneracy arises from the arbitrary rotation of a given convection solution in a spherical shell.

It is well known that solutions of the linear convective stability are characterized by l, the degree of a spherical harmonics Y_l^m [1]. The preferred value of l, denoted by l_c, and the radial structure of the linear solution can be determined by the linear stability analysis. It follows that there exists $(2l_c+1)$-fold degeneracy of the linear problem. Generally speaking, when the spherical shell is thick, $l_c=O(1)$, the removal or partial removal of the degeneracy is possible (e.g., [7]). However, when the thickness of the shell decreases, l_c increases and the corresponding nonlinear problem for removing or partially removing the $(2l_c+1)$-fold degeneracy becomes extremely complicated. Furthermore, there are fundamental differences between the cases with even and odd values of l_c.

It was first shown by Busse [7] (see also [10]) that the solvability conditions for the weakly nonlinear convection with $2\leqslant l_c\leqslant 6$ select a small number of steady convection patterns when the system is not self-adjoint. For example, he showed that the axisymmetric convection solution is preferred for $l_c=2$ while the tetrahedral solution is stable for $l_c=3$. The mathematical problem of two-dimensional pattern formation on a sphere without reference to the physical details of a system has been studied by a number of authors (e.g., [8,11,12]). Matthews [11,12] has recently made significant progress on the understanding of the spherical pattern problem for large values of l. He considered a two-dimensional variable W near a bifurcation point

$$W(\theta,\phi,t)=\sum_{m=-l}^{l} z_m(t)Y_l^m(\theta,\phi), \tag{1}$$

where z_m are in general complex and all the modes z_m have the same growth rate λ. The steady two-dimensional problem is then governed by the following $(2l+1)$ equations

*Electronic address: kzhang@ex.ac.uk

$$0 = \lambda z_m + \sum_{m_1=-l}^{l} \sum_{m_2=-l}^{l} c(m_1, m_2, m) z_{m_1} z_{m_2}, \tag{2}$$

where $c(m_1, m_2, m)$ are related to the Clebsch-Gordan coefficients. The existence and stability of the stationary solutions of Eq. (2) for even l up to $l=12$ were examined. Matthews [11,12] found that all bifurcating branches of stationary solutions to quadratic order are unstable, the axisymmetric state is never the preferred solution and the preferred solutions have icosahedral symmetry. In consequence, the higher-order terms, which are system dependent, play an essential role in determining the physically realizable patterns in spherical geometry. Matthews [11] also studied the Swift-Hohenberg model by numerical simulations using a pseudospectral method. Many different patterns, including axisymmetric and spiral solutions, were found.

This paper presents the first systematic study of three-dimensional spherical convection in a moderately thin spherical shell with $l_c = O(10)$ using fully three-dimensional numerical simulations. A number of new convection patterns in a spherical shell are found for the first time. The paper considers a Boussinesq fluid of uniform viscosity ν confined in a spherical shell bounded by two concentric spherical surfaces of inner radius r_i and outer radius r_o which have nonslip velocity and isothermal temperature boundary conditions. Convective motions in the spherical shell are driven by a spherically symmetric gravity force in connection with a spherically symmetric distribution of heat sources, a well-known convection model proposed by Chandrasekhar [1]. It is significant to note that the convection problem in a nonrotating spherical shell is self-adjoint. In comparison with rotating spherical convection in which the Coriolis force breaks spherical symmetry (e.g., [13–15]) and results in a strong zonal flow (e.g., [16–18]), an essential feature of nonrotating spherical convection is the high multiplicity of stable nonlinear solutions near its bifurcation point which is the focus of this paper.

The remainder of the paper is organized as follows. After discussing the mathematical formulation of thermal convection in Sec. II, the linear stability problem is discussed in Sec. III. The results of nonlinear convection are presented in Sec. IV. Section V closes the paper with a brief summary and some remarks.

II. MODEL AND MATHEMATICAL FORMULATION

We consider a Boussinesq fluid with constant thermal diffusivity κ, thermal expansion coefficient α, and kinematic viscosity ν. The Boussinesq fluid is confined in the spherical shell of the inner radius r_i and the outer radius r_o and is in the presence of its own gravitational field

$$\mathbf{g} = -\gamma \mathbf{r}, \tag{3}$$

where γ is a positive constant and $\mathbf{r}$ is the position vector with the origin at the center of the spherical shell. A well-known heating model [1] is adopted, in which the basic unstable conducting temperature gradient,

$$\nabla T_s(r) = -\beta \mathbf{r}, \tag{4}$$

where β is a positive constant, is produced by a uniform distribution of heat sources in the whole spherical system. The problem of thermal convection in a spherical shell is then governed by the following three equations [1]:

$$\frac{\partial \mathbf{u}}{\partial t} + \mathbf{u} \cdot \nabla \mathbf{u} = -\frac{1}{\rho} \nabla p + \gamma \alpha \Theta \mathbf{r} + \nu \nabla^2 \mathbf{u}, \tag{5}$$

$$\frac{\partial \Theta}{\partial t} + \mathbf{u} \cdot \nabla \Theta = \beta \mathbf{u} \cdot \mathbf{r} + \kappa \nabla^2 \Theta, \tag{6}$$

$$\nabla \cdot \mathbf{u} = 0, \tag{7}$$

where t is time, ρ is the fluid density, Θ represents the deviation of the temperature from its static distribution $T_s(r)$, p is the total pressure, and $\mathbf{u}$ is the three-dimensional velocity field, $\mathbf{u} = (u_r, u_\theta, u_\phi)$ in spherical polar coordinates (r, θ, ϕ) with $(\hat{\mathbf{r}}, \hat{\boldsymbol{\theta}}, \hat{\boldsymbol{\phi}})$ denoting the corresponding unit vectors. In Eq. (5), the term $\alpha\gamma\Theta\mathbf{r}$ represents the buoyancy force that drives thermal convection and provides a coupling to the heat equation (6).

We shall employ the thickness of the spherical shell $d = (r_o - r_i)$ as the length scale, d^2/ν as the unit of time, and $\beta d^2 \nu/\kappa$ as the unit of temperature fluctuation of the system, which lead to the dimensionless equations

$$\frac{\partial \mathbf{u}}{\partial t} + \mathbf{u} \cdot \nabla \mathbf{u} = -\nabla p + R\Theta \mathbf{r} + \nabla^2 \mathbf{u}, \tag{8}$$

$$\mathrm{Pr} \frac{\partial \Theta}{\partial t} + \mathbf{u} \cdot \nabla \Theta = \mathbf{u} \cdot \mathbf{r} + \nabla^2 \Theta, \tag{9}$$

$$\nabla \cdot \mathbf{u} = 0, \tag{10}$$

where the two nondimensional parameters, the Rayleigh number R and the Prandtl number Pr, are defined as

$$R = \frac{\alpha \beta \gamma d^6}{\nu \kappa}, \quad \mathrm{Pr} = \frac{\nu}{\kappa}.$$

All the variables in the rest of the paper will be nondimensional.

The velocity boundary conditions are nonslip and impenetrable, which give

$$\hat{\boldsymbol{\phi}} \cdot \mathbf{u} = \hat{\boldsymbol{\theta}} \cdot \mathbf{u} = \hat{\mathbf{r}} \cdot \mathbf{u} = 0 \tag{11}$$

at the inner and outer bounding spherical surface. Perfect thermally conducting boundaries impose the condition

$$\Theta = 0 \quad \text{at} \quad r = r_i, \quad r = r_o. \tag{12}$$

The nonlinear convection is solved by using a three-dimensional finite-difference method.

III. LINEAR CONVECTIVE STABILITY AND DEGENERACY

It is well known that the principle of exchange stability is valid for the onset of thermal convection in a nonrotating

spherical shell [1]. We therefore assume that $\partial/\partial t=0$, leading to the following equations for the linear stability problem:

$$0 = -\nabla p_0 + R_0\Theta_0\mathbf{r} + \nabla^2\mathbf{u}_0, \tag{13}$$

$$0 = \mathbf{u}_0\cdot\mathbf{r} + \nabla^2\Theta_0, \tag{14}$$

$$\boldsymbol{\nabla}\cdot\mathbf{u}_0 = 0. \tag{15}$$

The above linear system allows one to express the velocity $\mathbf{u}_0$ in the form

$$\mathbf{u} = \nabla\times\nabla\times(\mathbf{r}v_0), \tag{16}$$

i.e., the toroidal flow of convection vanishes in the linear problem. Substitution of Eq. (16) into Eqs. (13) and (14) and application of operator $\mathbf{r}\cdot\boldsymbol{\nabla}\times\nabla$ onto Eq. (13) yield

$$0 = \nabla^2\mathcal{L}\nabla^2 v_0 - R_0\mathcal{L}\Theta_0, \tag{17}$$

$$0 = \mathcal{L}v_0 + \nabla^2\Theta_0, \tag{18}$$

where $\mathcal{L}$ is given by

$$\mathcal{L} = -r^2\nabla^2 + \frac{\partial}{\partial r}r^2\frac{\partial}{\partial r}.$$

At the onset of spherical convection, the general linear solution may be written in the form

$$v_0 = \sum_{m=0}^{m=l} f_l(r)(C_m\cos m\phi + S_m\sin m\phi)P_l^m(\cos\theta), \tag{19}$$

$$\Theta = \sum_{m=0}^{m=l} g_l(r)(C_m\cos m\phi + S_m\sin m\phi)P_l^m(\cos\theta), \tag{20}$$

where $f_l(r)$ and $g_l(r)$ represent the radial eigenfunctions, $P_l^m(\cos\theta)$ denotes standard spherical harmonics of degree l, C_m, $m=0,1,2,\ldots,l$ and S_m, $m=1,2,3,\ldots,l$, are $(2l+1)$ undetermined coefficients. The linear stability problem then becomes

$$\left\{\left[\frac{1}{r}\frac{d^2}{dr^2}r - \frac{l(l+1)}{r^2}\right]^3 + l(l+1)R_0\right\}f_l(r) = 0, \tag{21}$$

$$g_l(r) = \frac{1}{R_0}\left[\frac{1}{r}\frac{d^2}{dr^2}r - \frac{l(l+1)}{r^2}\right]^2 f_l(r), \tag{22}$$

which subject to the boundary conditions

$$f_l = \frac{df_l}{dr} = \frac{d^2f_l}{dr^2} = 0 \tag{23}$$

at the two spherical bounding surfaces of the shell $r=r_i$ and $r=r_o$. The eigenvalue problem defined by Eqs. (21) and (23) can be readily solved by a shooting method. Some results are shown in Fig. 1 for two different aspect ratios of $\eta=r_i/r_o$. For a moderately thin spherical shell $\eta=0.847$, the critical Rayleigh number R_c, the lowest Rayleigh number required to excite convection, is located at $l_c=18$ and its neighboring values are given in Table I.

An important feature of the linear convection is its degeneracy. While the critical value of l and the radial structure of the flow, $g_l(r)$ and $f_l(r)$, are determined by the linear stability analysis, the $(2l+1)$ coefficients, C_m, $m=0,1,\ldots,l$ and S_m, $m=1,\ldots,l$, remain arbitrary, indicating that there exists the $(2l+1)$-fold degeneracy of the linear convection.

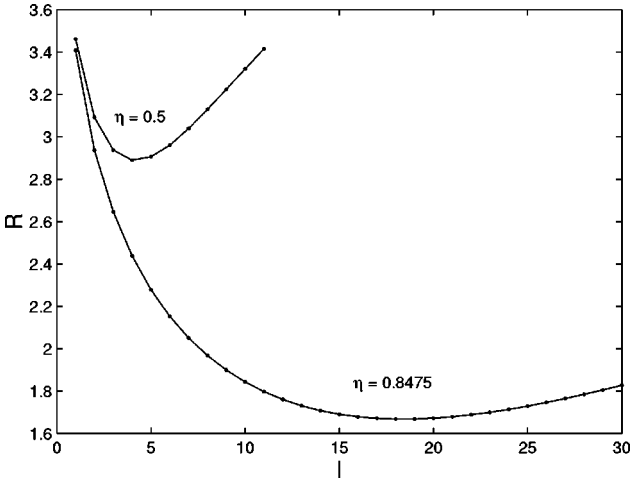

FIG. 1. The marginal Rayleigh number R_0 is shown as a function of l for two different values of $\eta=r_i/r_o$.

A complete or partial elimination of the $(2l+1)$-fold degeneracy by nonlinearity for the three-dimensional spherical convection proves and remains to be a mathematically challenging task. Both the number and spatial structure of the stable multiple three-dimensional convection in a spherical shell near the onset of convection represent an unsolved theoretical problem, in particular, when l is moderately large. This paper attempts to demonstrate, through careful three-dimensional numerical simulations, the existence and stability of multiple nonlinear convection solutions in a moderately thin shell with $\eta=0.847(l_c=18)$ characterized by a 37-fold degeneracy.

IV. MULTIPLICITY OF NONLINEAR SPHERICAL CONVECTION

A. Initial conditions for simulations

The linear analysis suggests that there exist multiple nonlinear solutions near the onset of thermal convection in a spherical shell. An important question is how to find these

TABLE I. The values of the marginal Rayleigh number R are shown as a function of l at the onset of convection for $\eta=0.847$. The most unstable convection mode is characterized by $l_c=18$ with the critical Rayleigh number $R_c=46.65$.

$(l,\ R_0)$	$(l,\ R_0)$
(14, 51.10)	(20, 47.10)
(15, 49.13)	(21, 47.82)
(16, 47.80)	(22, 48.85)
(17, 47.00)	(23, 50.17)
(**18**, **46.65**)	(24, 51.78)
(19, 46.70)	(25, 53.66)

different nonlinear convection solutions at the same parameters numerically. One effective way of obtaining multiple nonlinear solutions is to treat the usually steady convection problem as an initial-value problem, starting numerical integration of the system from carefully chosen different initial conditions. We employ the following parameterized initial condition

$$\mathbf{u}_0 = \frac{1}{r}\mathcal{L}\Psi\hat{\mathbf{r}} + \frac{1}{r}\frac{\partial}{\partial\theta}\left[\frac{\partial}{\partial r}(r\Psi)\right]\hat{\boldsymbol{\theta}} + \frac{1}{r\sin\theta}\frac{\partial}{\partial\phi}\left[\frac{\partial}{\partial r}(r\Psi)\right]\hat{\boldsymbol{\phi}}. \tag{24}$$

Here Ψ is given by

$$\Psi = [Y_l^m(\theta,\phi) + qY_n^j(\theta,\phi)]\frac{1}{r}\sin^2\pi(r-r_i), \tag{25}$$

where l, m, q, n, and j are the parameters of the initial condition. For example, when we choose $q=0$ and $l=18$ with different values of m, we start our numerical simulations of three-dimensional convection from different spherical harmonics of the same degree $l=18$ with the same radial structure but different spherical structures.

It usually takes a few viscous diffusion times for a nonlinear simulation to reach its stationary state. Dependent upon the parameter of a nonlinear convection, our simulations typically run about 5–60 viscous diffusion units. We shall focus on the case $(R-R_c)/R_c=0.28$ throughout the paper with Pr=7.0 (water at room temperature) and other values of Pr. In other words, we only consider the weakly nonlinear convection at the same Rayleigh number $[(R-R_c)/R_c=0.28]$ near the onset of convection, in attempting to obtain multiple nonlinear convection solutions at the exact same parameters of the problem.

B. Equatorially symmetric convection

There exist different parities of convection solutions with respect to the equatorial plane of a spherical shell. An equatorially symmetric convection is characterized by the symmetry property

$$(u_\theta, u_\phi, u_r)(\theta,\phi,r) = (-u_\theta, u_\phi, -u_r)(\pi-\theta, \phi+2\pi/m, r). \tag{26}$$

When $m=0$, the convection is axisymmetric, independent of the azimuthal angle ϕ in an appropriate spherical polar coordinate system. It is important to note that the position of a pole or an equator in our convection system is arbitrary because of orientational degeneracy of the problem. When we refer to an equatorial symmetry or an equator, we always imply that it is in an appropriately chosen spherical coordinate system. In fact, the position of a pole is largely determined by the spatial structure of an initial condition used in our numerical simulations. If an initial condition is equatorially symmetric, the corresponding nonlinear convection usually remains to be equatorially symmetric. We shall discuss below which and how different initial conditions result in multiple spherical nonlinear patterns near the onset of convection.

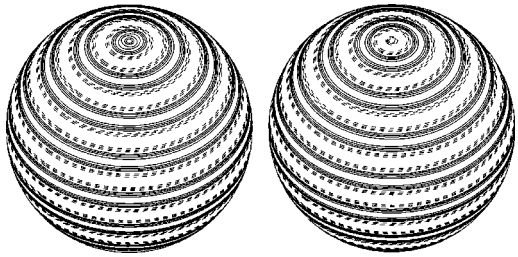

FIG. 2. Contours of radial flow u_r at the middle surface of the spherical shell for Pr=7.0. The solution shown on the left panel starts with the initial condition $\Psi(q=0,l=18,m=0)$ while the right panel starts with the initial condition $\Psi(q=0,l=18,m=10)$. The pattern is viewed from 45° from the north pole. Dashed contours indicate radially inward flow $u_r<0$ and solid contours correspond to radially outward flow $u_r>0$.

(1) The initial condition $\Psi(q=0,l=18,m=0)$. This azimuthally axisymmetric, equatorially symmetric initial condition leads to an axisymmetric stationary convection which is shown in Fig. 2 (left panel). Note that the convective flow arises from the polar regions (i.e., $u_r>0$ at $\theta=0,\pi$). The convection pattern on a spherical surface is essentially described by a single spherical harmonics $Y_{18}^0(\theta,\phi)$, indicating the stationary bifurcation from the linear solution given by $l=18$, $C_0=1$, $C_m=0, m=1,\ldots,l$ and $S_m=0, m=1,\ldots,l$ exists and is stable.

(2) The initial condition $\Psi(q=0,l=18,m=2)$. This azimuthally periodic, with the azimuthal wave number $m=2$, and equatorially symmetric initial condition leads to a stationary azimuthally periodic convection with $m=2$ which is shown in Fig. 3. The convection pattern in a spherical surface is described by a single spherical harmonics $Y_{18}^2(\theta,\phi)$, indicating the existence and stability of the bifurcation from the corresponding linear solution $Y_{18}^2(\theta,\phi)f_{18}(r)$.

(3) The initial condition $\Psi(q=0,l=18,m=4)$. This azimuthally periodic, with the azimuthal wave number $m=4$, and equatorially symmetric initial condition leads to a stationary azimuthally periodic convection with $m=4$ which is shown in Fig. 4. Similar to the case $\Psi(q=0,l=18,m=2)$, the equatorially symmetric convection on a spherical surface is largely described by a single spherical harmonics $Y_{18}^4(\theta,\phi)$.

(4) The initial condition $\Psi(q=0,l=18,m=6)$. In contrast to the previous cases $\Psi(q=0,l=18,m=2)$ and $\Psi(q=0,l=18,m=4)$, this azimuthally periodic, with the azimuthal

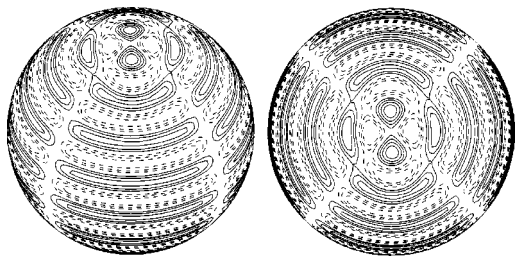

FIG. 3. Contours of radial flow u_r at the middle surface of the spherical shell for Pr=7.0 with the initial condition $\Psi(q=0,l=18,m=2)$. On the left panel, we view it from 45° from the north pole while the right panel is viewed from the south pole.

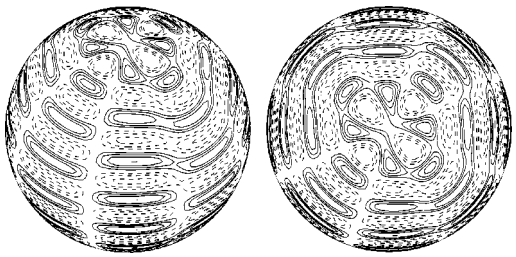

FIG. 4. Contours of radial flow u_r at the middle surface of the spherical shell for Pr=7.0 with the initial condition $\Psi(q=0,l=18,m=4)$. On the left panel, we view it from 45° from the north pole while the right panel is viewed from the south pole.

wave number $m=6$, and equatorially symmetric initial condition leads to an axisymmetric stationary convection which is eventually the same as that obtained from the simulation commencing from $\Psi(q=0,l=18,m=0)$, which is shown on the left panel of Fig. 2. It suggests that the bifurcation from the linear solution described by $Y_{18}^{6}(\theta,\phi)f_{18}(r)$ does not exist or is unstable.

(5) The initial condition $\Psi(q=0,l=18,m=8)$. This azimuthally periodic, with the azimuthal wave number $m=8$, and equatorially symmetric initial condition leads to a stationary, azimuthally nonperiodic, equatorially symmetric convection which is shown in Fig. 5. There are a number of small convection cells in the polar regions and the long convection rolls that are nearly parallel to the equator in the equatorial and lower latitudinal regions. While the equatorial symmetry of the convective flow is preserved, there is no azimuthal symmetry or periodicity comparing to the previous cases with the small-m initial conditions.

(6) The initial condition $\Psi(q=0,l=18,m=10)$. This azimuthally periodic, equatorially symmetric initial condition leads to an axisymmetric stationary convection which is shown in the right panel of Fig. 2. This axisymmetric solution is different from the case (1) with $\Psi(q=0,l=18,m=0)$ (left panel of Fig. 2) since the convective flow in this case descends in the polar regions (i.e., $u_r<0$ at $\theta=0,\pi$). But the convection pattern on a spherical surface is still mainly described by a single spherical harmonics $Y_{18}^{0}(\theta,\phi)$, indicating that there exist two different axisymmetric nonlinear solutions. It also suggests that the bifurcation from the linear solution described by $Y_{18}^{10}(\theta,\phi)f_{18}(r)$ is unstable or does not exist.

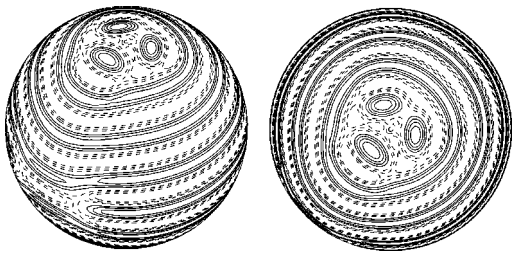

FIG. 5. Contours of radial flow u_r at the middle surface of the spherical shell for Pr=7.0 with the initial condition $\Psi(q=0,l=18,m=8)$. On the left panel, we view it from 45° from the north pole while the right panel is viewed from the south pole.

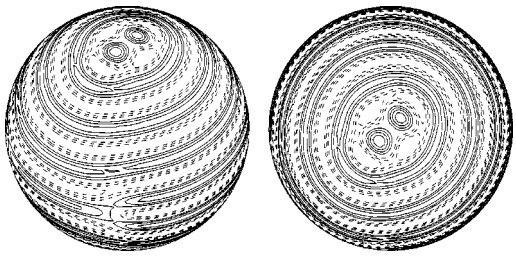

FIG. 6. Contours of radial flow u_r at the middle surface of the spherical shell for Pr=7.0 with the initial condition $\Psi(q=0,l=18,m=12)$. On the left panel, we view it from 45° from the north pole while the right panel is viewed from the south pole.

(7) The initial condition $\Psi(q=0,l=18,m=12)$. This azimuthally periodic, equatorially symmetric initial condition leads to a stationary, azimuthally nonperiodic, equatorially symmetric convection which is shown in Fig. 6. There are two small convection cells in the polar regions while the azimuthal structure of the nearly axisymmetric convection rolls in lower latitudes is modulated. It suggests that the bifurcation from the linear solution $Y_{18}^{12}(\theta,\phi)f_{18}(r)$ is unstable or does not exist.

(8) The initial condition $\Psi(q=0,l=18,m=14)$. This azimuthally nonaxisymmetric, equatorially symmetric initial condition leads to the axisymmetric stationary convection which is the same as that obtained using $\Psi(q=0,l=18,m=10)$ shown in the right panel of Fig. 2. It suggests that the bifurcation from the linear solution $Y_{18}^{14}(\theta,\phi)f_{18}(r)$ is unstable or does not exist.

(9) The initial condition $\Psi(q=0,l=18,m=16)$. This azimuthally periodic, equatorially symmetric initial condition leads to the axisymmetric stationary convection which is the same as that obtained using $\Psi(q=0,l=18,m=0)$ shown in the left panel of Fig. 2, suggesting that the bifurcation from the linear solution described by $Y_{18}^{16}(\theta,\phi)f_{18}(r)$ is unstable or does not exist.

C. Equatorially asymmetric convection

An equatorially antisymmetric initial condition is characterized by the symmetry property

FIG. 7. Contours of radial flow u_r at the middle surface of the spherical shell for Pr=7.0 with the initial condition $\Psi(q=0,l=18,m=1)$. On the left panel, we view it from 45° from the north pole while the right panel is viewed from the south pole.

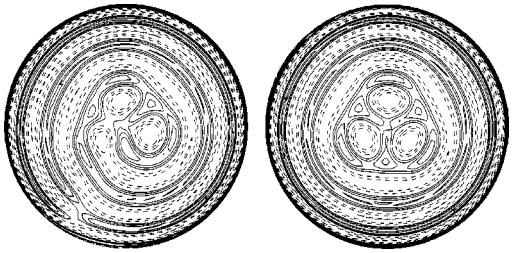

FIG. 8. Contours of radial flow u_r at the middle surface of the spherical shell for Pr=7.0 with the initial condition $\Psi(q=0, l=18, m=3)$. On the left panel, we view it from the north pole while the right panel is viewed from the south pole.

$$(u_\theta, u_\phi, u_r)(\theta, \phi, r) = (u_\theta, -u_\phi, u_r)(\pi - \theta, \phi + 2\pi/m, r) \tag{27}$$

in an appropriate spherical polar coordinate. Again it is of importance to notice that the position of a pole ($\theta=0$, or π) is arbitrary because of orientational degeneracy of the problem. If an initial condition is equatorially antisymmetric, the corresponding nonlinear convection usually remains to be equatorially asymmetric.

(1) The initial condition $\Psi(q=0, l=18, m=1)$. It should be noted that this initial condition represents a special case because of the particular symmetry property of $Y_{18}^1(\theta, \phi)$. The resulting convection pattern is displayed in Fig. 7. It indicates that the stationary convection bifurcating from the linear solution described by $Y_{18}^1(\theta, \phi) f_{18}(r)$ exists and is stable.

(2) The initial condition $\Psi(q=0, l=18, m=3)$. This azimuthally periodic, equatorially antisymmetric initial condition leads to azimuthally nonperiodic, equatorially asymmetric, stationary convection. There is a broken spiral roll in the northern hemisphere while the azimuthal wave number $m=3$ can be clearly seen in the southern polar region. The resulting flow pattern is shown in Fig. 8. The convective flow possesses neither equatorial nor azimuthal symmetries, suggesting that the stationary convection bifurcating from the linear solution described by $Y_{18}^3(\theta, \phi) f_{18}(r)$ does not exist or is unstable.

(3) The initial condition $\Psi(q=0, l=18, m=5)$. This azimuthally periodic, equatorially antisymmetric initial condition leads to equatorially asymmetric, stationary convection, which is shown in Fig. 9. It is apparent that convection in the

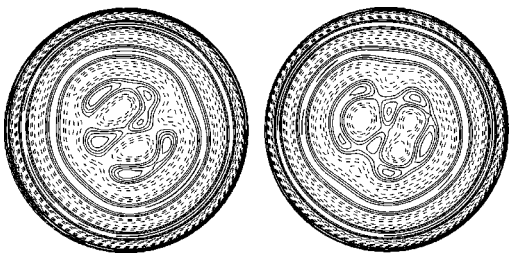

FIG. 9. Contours of radial flow u_r at the middle surface of the spherical shell for Pr=7.0 with the initial condition $\Psi(q=0, l=18, m=5)$. On the left panel, we view it from the north pole while the right panel is viewed from the south pole.

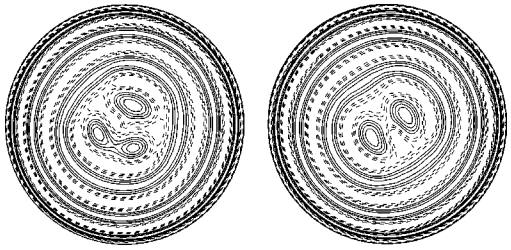

FIG. 10. Contours of radial flow u_r at the middle surface of the spherical shell for Pr=7.0 with the initial condition $\Psi(q=0, l=18, m=7)$. In the left panel, we view it from the north pole while the right panel is viewed from the south pole.

form of long rolls circulating the whole sphere can be readily formed. However, these long rolls can be only easily formed in the equatorial region while they cannot be readily placed in the polar regions because of spherical topology. As a result, many convection patterns have similar characteristics in the equatorial region but the flow structure in the polar regions, which is usually complicated, highly depends upon the spatial structure of an initial condition.

(4) The initial condition $\Psi(q=0, l=18, m=7)$. This azimuthally periodic, equatorially antisymmetric initial condition leads to azimuthally nonperiodic, equatorially asymmetric, stationary convection, which is shown in Fig. 10. Again there are several long rolls circulating the equatorial region while a number of small irregular cells are formed in the two polar regions.

(5) The initial condition $\Psi(q=0, l=18, m=9)$. This azimuthally periodic, equatorially antisymmetric initial condition leads to equatorially asymmetric, azimuthally nonperiodic stationary convection, which is shown in Fig. 11. In the southern hemisphere, there exists a long spiral roll while the convection is nearly axisymmetric in the northern hemisphere.

(6) The initial condition $\Psi(q=0, l=18, m=11)$. This azimuthally periodic, equatorially antisymmetric initial condition leads to equatorially asymmetric, azimuthally nonperiodic stationary convection, which is shown in Fig. 12. Again it is the flow structure in the polar regions that is distinctly different from those using different initial conditions.

(7) The initial condition $\Psi(q=0, l=18, m=13)$. This azimuthally periodic, equatorially antisymmetric initial condition leads to equatorially asymmetric, azimuthally nonperiodic, stationary convection which is shown in Fig. 13.

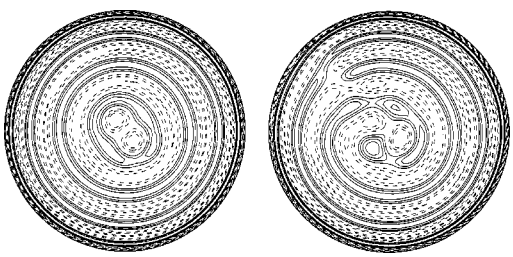

FIG. 11. Contours of radial flow u_r at the middle surface of the spherical shell for Pr=7.0 with the initial condition $\Psi(q=0, l=18, m=9)$. On the left panel, we view it from the north pole while the right panel is viewed from the south pole.

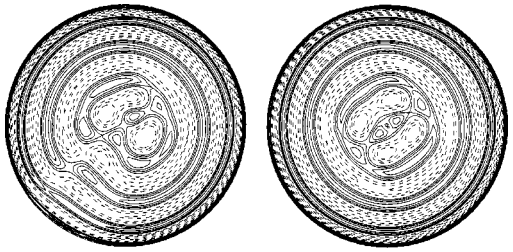

FIG. 12. Contours of radial flow u_r at the middle surface of the spherical shell for Pr=7.0 with the initial condition $\Psi(q=0,l=18,m=11)$. On the left panel, we view it from the north pole while the right panel is viewed from the south pole.

Similar to the previous cases, the long equatorial convection rolls divide the flows into the two hemispherical regions with little communication between them.

(8) The initial condition $\Psi(q=0,l=18,m=15)$. This azimuthally periodic, equatorially antisymmetric initial condition leads to equatorially asymmetric, azimuthally nonperiodic, stationary convection shown in Fig. 14. This case is again similar to the previous cases using smaller azimuthal wave numbers as the initial conditions.

(9) The initial condition $\Psi(q=0,l=18,m=17)$. This azimuthally periodic, equatorially antisymmetric initial condition leads to equatorially asymmetric, azimuthally nonperiodic, stationary convection which is shown in Fig. 15. In comparison to the equatorially symmetric initial conditions, all the equatorially antisymmetric initial conditions (except for the special case $m=1$) result in spherical convection patterns that have neither the equatorial nor azimuthal symmetries and that cannot be simply described by a single or a combination of a small number of spherical harmonics. This is mainly attributable to the intricate structure of convection in the polar regions. In some ways, convection in the two polar regions resembles the extensively studied plane-layer problem but with different horizontal boundary conditions. In the present problem, the long rolls circulating the whole sphere in the equatorial region eventually impose a horizontal boundary condition for the polar convection and hence determine the structure of the flow in the polar regions.

D. Equatorially mixed-symmetric initial conditions

It is practically impossible to simulate all the possible combinations of equatorially mixed-symmetric initial conditions with different values of l and j in Eq. (25). We therefore focus on the highly robust pattern of spherical thermal convection resulting from the mixed-symmetric initial condition $\Psi(q=1,l=18,j=m=1,n=19)$. In this case, the steady nonlinear equilibrium of spherical convection is always described by a single, giant spiral roll extending from the north pole to the south pole without defects and covering the whole spherical surface. This particular spherical spiral roll was first discovered at Pr=7 reported in a short Rapid Communication [19].

We have extended the previous analysis to a large range of Pr in $O(10^{-2}) \leqslant \mathrm{Pr} \leqslant 100$. It is found that the spherical convection pattern in the form of a single giant spiral roll is robust, stationary, and stable for the whole range $0.1 \leqslant \mathrm{Pr} \leqslant 100$. Kinetic energies of the flow and the corresponding styles of convection for various values of Pr are shown in Table II. Although the kinetic energy of convection changes enormously for different values of Pr, the pattern of convection remains nearly unchanged for $0.1 \leqslant \mathrm{Pr} \leqslant 100$. Two typical examples of the convective flow are shown in Fig. 16 for Pr=100 and Pr=0.1, respectively, showing a stationary, single, giant spiral roll covering the whole spherical surface. It is worth noting that the position of the poles at which the spiral roll starts or ends is arbitrary because of orientational degeneracy.

For smaller values of $\mathrm{Pr} < 0.1$, the nonlinear thermal convection becomes weakly time-dependent and the single long spiral roll breaks up into four shorter spiral rolls located in the equatorial and middle-latitude regions. The way the four spiral rolls are connected and vary with time is shown in Fig. 17 for four different instants and its time-dependent kinetic energy is displayed in Fig. 18. A very small time-step is

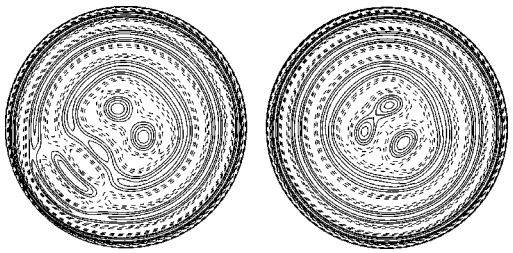

FIG. 13. Contours of radial flow u_r at the middle surface of the spherical shell for Pr=7.0 with an initial condition $\Psi(q=0,l=18,m=13)$. On the left panel, we view it from the north pole while the right panel is viewed from the south pole.

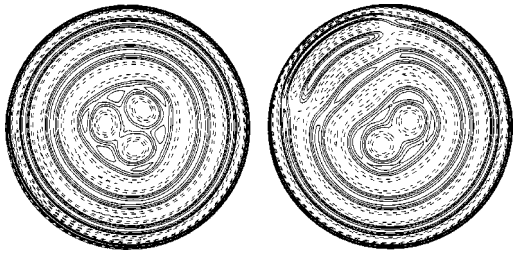

FIG. 14. Contours of radial flow u_r at the middle surface of the spherical shell for Pr=7.0 with the initial condition $\Psi(q=0,l=18,m=15)$. On the left panel, we view it from the north pole while the right panel is viewed from the south pole.

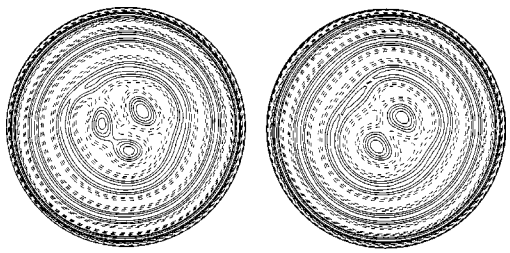

FIG. 15. Contours of radial flow u_r at the middle surface of the spherical shell for Pr=7.0 with the initial condition $\Psi(q=0,l=18,m=17)$. On the left panel, we view it from the north pole while the right panel is viewed from the south pole.

TABLE II. The kinetic energies of convection are shown as a function of Pr with the mixed-symmetry initial condition.

Pr	Kinetic energy	Convection pattern
100	0.13	steady, single giant spherical spiral
7	152.8	steady, single giant spherical spiral
5	299.6	steady, single giant spherical spiral
3	829.4	steady, single giant spherical spiral
1	7383.9	steady, single giant spherical spiral
0.7	14 787	steady, single giant spherical spiral
0.3	71 203	steady, single giant spherical spiral
0.1	413 098	steady, single giant spherical spiral
0.05	$\approx 4.6\times 10^5$	time-dependent, multiple shorter spirals

required for simulating small-Prandtl-number convection, making the systematic investigation of the behavior of small-Pr convection numerically difficult.

V. SUMMARY AND REMARKS

This is the first paper that investigates the multiplicity of nonlinear convection in a moderately thin spherical shell and demonstrates numerically the existence of a large number of different patterns of spherical convection at the exact same parameter in the vicinity of convective instability. In particular, a single, giant, perfect spherical spiral roll is discovered to be stable and robust in a wide range of the Prandtl number Pr. In contrast to nonlinear patterns in other geometries like a plane layer or a cylinder, the long steady roll, guided by spherical topology, circuiting and covering the whole spherical surface, represents the unique characteristic of spherical-geometry convection.

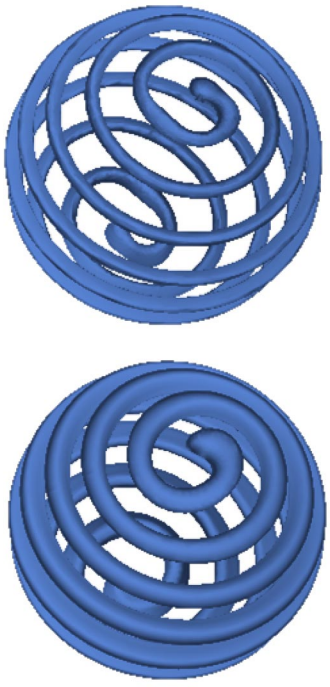

FIG. 16. Steady convection in the form of a stationary giant spherical spiral roll obtained for Pr=100 (upper) and Pr =0.1 (lower).

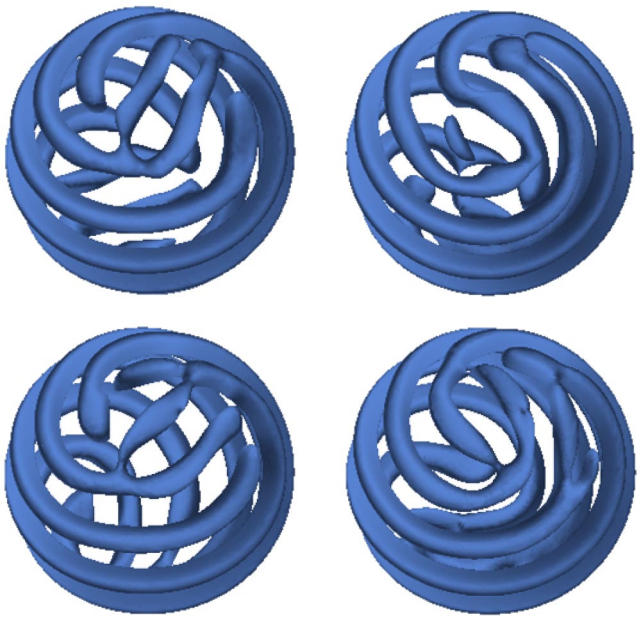

FIG. 17. Contours of radial flow u_r at the middle surface of the spherical shell for Pr=0.05 at four different instants at $t=6$, 7, 8, and 9.

The mathematical problem for nonlinear spherical convection associated with a large l is not well understood. Our theoretical knowledge for the existence and stability of weakly nonlinear thermal convection in a moderately thin spherical shell is highly limited. We have chosen to tackle the problem by performing systematic simulations of nonlinear thermal convection using different initial conditions while keeping the other parameters unchanged. By the nature of the method, it is certain that our numerical simulations cannot reveal all the possible stable nonlinear convection solutions. Nevertheless, on the basis of the current simula-

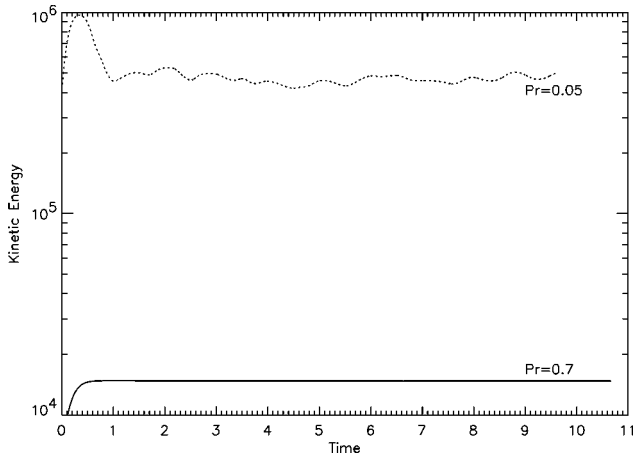

FIG. 18. The kinematic energies of convection are shown as a function of time for Pr=0.7 (a single long spiral roll) and Pr =0.05 (multiple shorter spirals).

tions, we propose the following conjectures for nonlinear spherical convection near the critical point for $\mathrm{Pr}=O(1)$ in a moderately thin spherical shell.

(i) Steady nonlinear convection with an azimuthal axisymmetry ($m=0$) and an equatorial symmetry bifurcating from $Y_{18}^{0}(\theta,\phi)f_{18}(r)$ exists and is stable. There are two different axisymmetric stable convection solutions: one has the flow out of the two polar regions (i.e., $u_r>0$ at $\theta=0$ and π); the another has the flow into the two polar regions (i.e., $u_r<0$ at $\theta=0$ and π). Note that, if a particular $\mathbf{u}_0$ is a solution of the problem, $-\mathbf{u}_0$ cannot be also a solution of the nonlinear problem.

(ii) Steady nonlinear convection solutions bifurcating from the linear solutions $Y_{18}^{m}(\theta,\phi)f_{18}(r)$ with $m=1,2,4$ exist and are stable.

(iii) All steady nonlinear solutions bifurcating from $Y_{18}^{m}(\theta,\phi)f_{18}(r)$ with $m=3,5,6,7,8,\ldots,17$ are unstable or do not exist.

It should be noted that our three-dimensional spherical convection has fundamental differences from the problem described by two-dimensional quadratic equations (2) on a sphere, even though the critical value l for the onset of convection is given by an even value. This is because our problem of convection in a spherical shell (both the governing equations and the adjoint boundary conditions) is self-adjoint [7]. For illustrating this important point, we discuss briefly the derivation of equations like Eq. (2) in the context of thermal spherical convection. We shall assume that the weakly nonlinear convection is stationary. Introduce the power series

$$R = R_0 + \epsilon R_1 + \epsilon^2 R_2, \quad v = \varepsilon v_0 + \varepsilon^2 v_1 + \varepsilon^3 v_2, \ldots, \quad (28)$$

where ϵ is a small expansion parameter, the amplitude of thermal convection. The leading-order problem gives rise to the onset of convection the result of which is shown in Table I. In the next-order problem, it can be shown that $R_1=0$ and that all coefficients for the quadratic terms in equations like Eq. (2) are identically zero when the convection problem is self-adjoint and when the radial structure of the convection (i.e., a three-dimensional problem in a spherical shell rather than a two-dimensional problem on a sphere) has been taken into account. It follows that the higher-order terms play an essential role in the present weakly nonlinear convection problem. However, the corresponding theoretical problem near the bifurcation point becomes extremely complicated and is not well understood, particularly in a moderately thin spherical shell.

ACKNOWLEDGMENTS

L.L. and K.Z. were supported by NERC and PPARC grants, P.Z. and K.Z. were supported by Leverhulme Trust, and X.L. was supported by NSFC grants.

[1] S. Chandrasekhar, *Hydrodynamic and Hydromagnetic Stability* (Clarendon Press, Oxford, 1961).
[2] G. Schubert, Annu. Rev. Fluid Mech. **7**, 289 (1979).
[3] K. Zhang and F. H. Busse, Phys. Earth Planet. Inter. **104**, 283 (1997).
[4] D. Gubbins and J. Bloxham, Nature (London) **325**, 509 (1987).
[5] J. Bloxham, Nature (London) **405**, 63 (2000).
[6] K. Zhang and D. Gubbins, J. Fluid Mech. **250**, 209 (1993).
[7] F. H. Busse, J. Fluid Mech. **72**, 67 (1975).
[8] P. Chossat, SIAM (Soc. Ind. Appl. Math.) J. Appl. Math. **37**, 627 (1979).
[9] G. Schubert and A. Zebib, Geophys. Astrophys. Fluid Dyn. **15**, 65 (1980).
[10] F. H. Busse and N. Riahi, J. Fluid Mech. 283 (1982).
[11] P. C. Matthews, Phys. Rev. E **67**, 036206 (2003).
[12] P. C. Matthews, Nonlinearity **16**, 1449 (2003).
[13] F. H. Busse, Phys. Fluids **14** 1301 (2002).
[14] A. M. Dormy, A. M. Soward, C. A. Jones, D. Jault, and P. Cardin, J. Fluid Mech. **501**, 43 (2004).
[15] K. Zhang and F. H. Busse, Adv. Fluid Mech. **20**, 17 (1998).
[16] A. Tilgner and F. H. Busse, J. Fluid Mech. **332**, 359 (1997).
[17] I. Sumita and P. L. Olson, Phys. Earth Planet. Inter. **117**, 153 (2000).
[18] J. M. Aurnou and P. L. Olson, Geophys. Res. Lett. **28**, 2557 (2001).
[19] P. Zhang, X. Liao, and K. Zhang, Phys. Rev. E **66**, 055203 (2002).